Unenhanced Dynamic MR Angiography: High Spatial and Temporal Resolution by Using True FISP–based Spin Tagging with Alternating Radiofrequency[1]

Lirong Yan, BS
Sumei Wang, MD
Yan Zhuo, MS
Ronald L. Wolf, MD, PhD
Michael F. Stiefel, MD, PhD
Jing An, MD
Yongquan Ye, PhD
Qian Zhang, MD
Elias R. Melhem, MD, PhD
Danny J. J. Wang, PhD

Purpose: To present an unenhanced four-dimensional time-resolved dynamic magnetic resonance (MR) angiography technique with true fast imaging with steady-state precession–based spin tagging with alternating radiofrequency (STAR), also called TrueSTAR.

Materials and Methods: This study received Institutional Review Board approval and was HIPAA compliant. Informed consent was obtained from all study subjects. In eight healthy volunteers, the spatial and temporal resolution of the TrueSTAR technique were optimized. In another six healthy volunteers, the contrast-to-noise ratio (CNR) and signal-to-noise ratio (SNR) of the TrueSTAR dynamic MR angiography images were compared with those acquired by using a standard Look-Locker echo-planar technique by using the Wilcoxon signed rank test. Finally, one patient with an arteriovenous malformation (AVM) was studied by using this technique.

Results: The SNR and CNR of the TrueSTAR dynamic MR angiography images were 29% and 39% higher, respectively, compared with those acquired by using a standard Look-Locker echo-planar imaging sequence (both $P = .028$). In the AVM patient, TrueSTAR dynamic MR angiography delineated the dynamic course of labeled blood flowing through feeding arteries into the nidus and draining veins.

Conclusion: The results suggest that TrueSTAR is a promising unenhanced dynamic MR angiography technique for clinical evaluation of cerebrovascular disorders such as AVM, steno-occlusive disease, and aneurysm.

Supplemental material: *http://radiology.rsna.org/lookup/suppl/doi:10.1148/radiol.10091543/-/DC1*

[1] From the State Key Laboratory of Brain and Cognitive Science, Institute of Biophysics, Chinese Academy of Sciences, Beijing, China (L.Y., Y.Z., Y.Y.); Beijing MRI Center for Brain Research, Beijing, China (L.Y., Y.Z., Y.Y.); Departments of Radiology (S.W., R.L.W., M.F.S., E.R.M., D.J.J.W.) and Neurology (D.J.J.W.), University of Pennsylvania, Philadelphia, Pa; Siemens Mindit Magnetic Resonance, Shenzhen, China (J.A.); and Department of Neurosurgery, Beijing Tiantan Hospital, Beijing, China (Q.Z.). Received August 18, 2009; revision requested October 9; revision received November 19; accepted January 12, 2010; final version accepted January 25. Supported by the Ministry of Science and Technology of China (grants 2005CB522800 and 2004CB318101), National Nature Science Foundation of China (grant 30621004), Knowledge Innovation Program of the Chinese Academy of Sciences, Thrasher Research Fund, and American Recovery and Reinvestment Act (grant MH080892-S1). **Address correspondence to** D.J.J.W., Department of Neurology, Ahmanson-Lovelace Brain Mapping Center, University of California Los Angeles, 660 Charles E. Young Dr S, Los Angeles, CA 90095-7085 (e-mail: *jwang71@gmail.com*).

The evaluation of the dynamic flow patterns within the cerebral vasculature might be useful for a number of clinical indications, such as assessment of the collateral circulation in patients with cerebrovascular steno-occlusive disease, estimation of the degree of shunted blood flow in an arteriovenous malformation (AVM), and delineation of aberrant flow through a cerebral aneurysm (1–4). Intraarterial digital subtraction angiography is currently the reference standard for these indications, as it can provide images of the cerebral blood circulation with both high temporal and spatial resolution. The procedure, however, is invasive and requires the use of ionizing radiation, with its risks, and iodinated contrast agent, with its own risks of contrast agent reactions and contrast agent–induced nephropathy (5).

Recently, contrast agent–enhanced dynamic magnetic resonance (MR) angiography has received considerable attention and has been applied in the evaluation of the cerebral vasculature because of its ability to provide temporal information in addition to the otherwise static high spatial resolution of three-dimensional (3D) contrast-enhanced MR angiography (6–9). However, the temporal resolution in contrast-enhanced dynamic MR angiography is generally on the order of seconds, and the method requires intravenous injection of a contrast agent. As an alternative method without the use of contrast agents, dynamic MR angiography can be performed with pulsed arterial spin labeling in conjunction with a segmented turbo fast low-angle shot or a continuous Look-Locker sequence (10–13). The appealing feature of spin-labeling–based dynamic MR angiography is its high temporal resolution (on the order of tens of milliseconds); however, the spatial resolution and signal-to-noise ratio (SNR) of these techniques are not satisfactory because of the need for low flip angles and/or saturation effects that may occur with turbo fast low-angle shot and Look-Locker sequences.

True fast imaging with steady-state precession (FISP) imaging is a balanced steady-state free precession technique that offers high SNR and imaging efficiency and is ideal for blood vessel imaging because of the high signal intensity from blood, which has an intrinsically high T2/T1 ratio (14,15). The technique is also inherently flow compensated, thereby minimizing sensitivity to flow artifacts (16). In addition, true FISP has relatively low sensitivity to susceptibility artifacts (17). The goal of our study was to present an unenhanced four-dimensional time-resolved dynamic MR angiography technique (true FISP) that is based on spin tagging with alternating radiofrequency (STAR), also called TrueSTAR (18). The method lends itself well to clinical situations, as we demonstrated with a typical case of cerebral AVM.

Advances in Knowledge

- Time-resolved four-dimensional dynamic MR angiography can be achieved without contrast agents by combining spin-labeling methods with multiphase true fast imaging with steady-state precession (FISP) readout.
- This technique offers improved dynamic MR angiography image quality (29% increased signal-to-noise ratio, 39% increased contrast-to-noise ratio; both P = .028) compared with standard Look-Locker–based methods.

Materials and Methods

Study Population

This prospective study was approved by the Institutional Review Boards of the University of Pennsylvania and the Institute of Biophysics at the Chinese Academy of Sciences and was Health Insurance Portability and Accountability Act compliant. Written informed consent was obtained from all subjects prior to the MR examination. Fourteen healthy volunteers (mean age, 23 years ± 2 [standard deviation]; seven men and seven women) without neurologic illness and one patient who had been diagnosed with a cerebral AVM (29-year-old man) participated in our study. All imaging was performed on 3-T MR imagers (Tim Trio; Siemens, Erlangen, Germany) with a body coil as the transmitter and a 12-channel head array coil as the receiver.

Implications for Patient Care

- Spin-labeling methods and multiphase true FISP readout can be combined for unenhanced dynamic MR angiography for visualizing the dynamic flow pattern in arteriovenous malformation.
- This technique may be useful in the clinical evaluation of cerebrovascular steno-occlusive disease, as well as in the delineation of aberrant flow through an aneurysm.

MR Imaging of Healthy Volunteers

The TrueSTAR technique combines time-resolved arterial spin labeling with a segmented multiphase true FISP readout. In our study, the flow-sensitive alternating inversion recovery technique (19) was implemented for spin labeling. As shown in Figure 1, the pulse sequence diagram, immediately following a section-selective or nonselective hyperbolic secant inversion pulse, a train of 20 dummy radiofrequency

Published online
10.1148/radiol.10091543

Radiology 2010; 256:270–279

Abbreviations:
AVM = arteriovenous malformation
CNR = contrast-to-noise ratio
FISP = fast imaging with steady-state precession
MIP = maximum intensity projection
SNR = signal-to-noise ratio
STAR = spin tagging with alternating radiofrequency
3D = three-dimensional

Author contributions:
Guarantors of integrity of entire study, L.Y., Y.Z., D.J.J.W.; study concepts/study design or data acquisition or data analysis/interpretation, all authors; manuscript drafting or manuscript revision for important intellectual content, all authors; approval of final version of submitted manuscript, all authors; literature research, L.Y., S.W., Y.Z., R.L.W., Y.Y., D.J.J.W.; clinical studies, all authors; statistical analysis, L.Y., Y.Z., D.J.J.W.; and manuscript editing, L.Y., S.W., Y.Z., R.L.W., M.F.S., E.R.M., D.J.J.W.

Funding:
This research was supported by National Institutes of Health (grants MH080892, RR002305, and NS065292).

Authors stated no financial relationship to disclose.

Figure 1

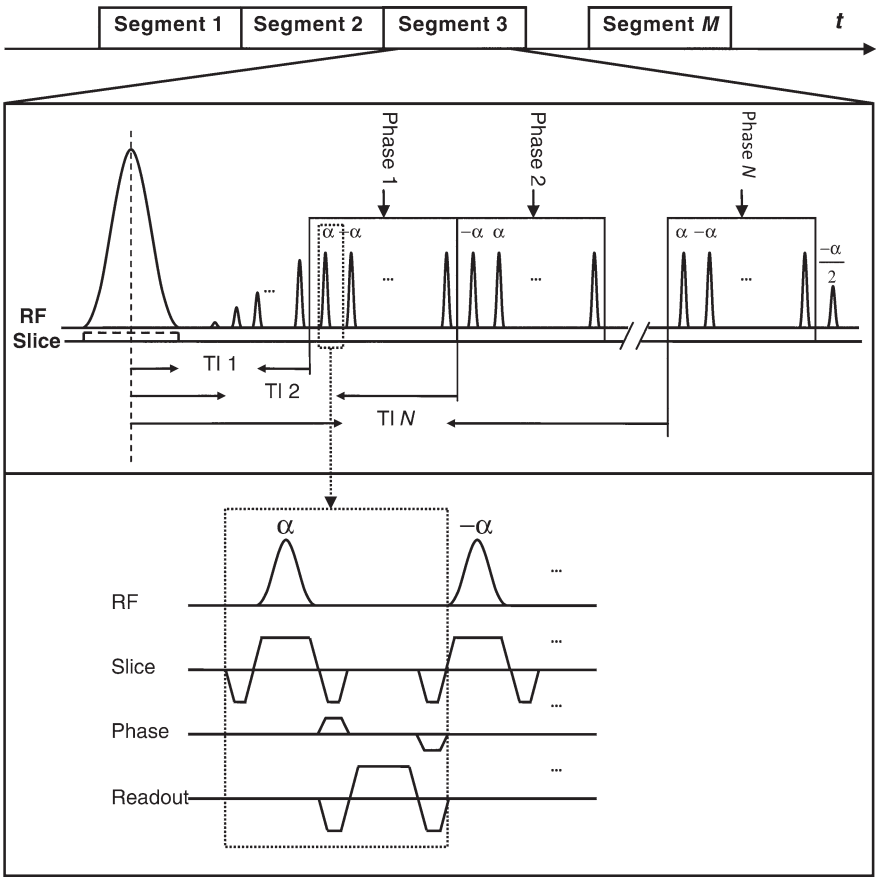

Figure 1: Pulse sequence diagram of TrueSTAR with flow-sensitive alternating inversion recovery for spin labeling. Layout of gradient and readout is shown in inset. α = flip angle, *RF* = radiofrequency, *TI* = inversion time.

pulses with Kaiser Bessel window ramp flip angles (ie, $\alpha/21$, $-2\alpha/21$, $3\alpha/21$, …, $-20\alpha/21$) was applied to minimize transient signal oscillations (20). The signal was then continuously acquired by a segmented multiphase true FISP readout with the $\pm\alpha$ radiofrequency pulse scheme with phase encoding advancing in a centric order. At the end of the true FISP readout, the magnetization was restored to the positive z-axis by using an $\alpha/2$ pulse. The series of TrueSTAR images were formed in a manner similar to cine MR imaging methods (ie, an image for an individual time frame was generated from multiple segmented acquisitions synchronized to the labeling pulse). In our study, 11–21 k-space lines were acquired per segment, resulting in a temporal resolution of 50–100 msec for each time frame image.

We conducted three consecutive experiments in healthy volunteers to optimize the TrueSTAR technique. Detailed imaging parameters are listed in Table 1. In all three experiments, images were acquired to cover the circle of Willis and associated main branches. The main purpose of experiment 1 was to determine the optimal gap between the labeling and imaging slab by measuring the arrival time of the labeling bolus as a function of the thickness of the selective inversion band. The thickness of the selective inversion pulse was set to five, 10, and 15 times the imaging section thickness (5 mm).

In experiment 2, we attempted to further improve the SNR (owing to volume excitation) and imaging resolution along the z-axis by using 3D TrueSTAR acquisitions. In part 2a, generalized autocalibrating partially parallel acquisition with an acceleration factor of two was applied to reduce the total imaging time to approximately 7 minutes while preserving a temporal resolution of 83 msec with 30 phases. To investigate the effects of cardiac pulsation on dynamic MR angiography images (21), we also performed pulse-gated (electrocardiographically gated) 3D cine TrueSTAR imaging in experiment 2b. Depending on the cardiac cycle, 10–15 phases of dynamic MR angiography images with a temporal resolution of 52 msec were acquired within approximately 6 minutes.

In experiment 3, the TrueSTAR technique was compared with a standard dynamic MR angiography method based on a Look-Locker echo-planar imaging sequence with closely matched parameters. Three flip angles (α = 20°, 40°, and 60°) were tested to investigate potential saturation effects in both techniques.

Patient Studies

One patient (29-year-old man) who had been diagnosed with an AVM was imaged with the 3D TrueSTAR protocol without the pulse trigger. The imaging parameters were identical to the protocol used in experiment 2a (see Table 1), except that the section thickness was set to 3 mm to cover the whole AVM lesion (slab thickness = 3 × 20 = 60 mm). Conventional MR sequences included axial T1-weighted 3D magnetization prepared rapid acquisition gradient-echo (1760/3.1; inversion time, 950 msec; spatial resolution, 1 × 1 × 1 mm), T2-weighted fast spin-echo (4000/87; spatial resolution, 0.43 × 0.43 × 4.8 mm), and time-of-flight MR angiography (33/3.86; spatial resolution, 0.57 × 0.57 × 0.65 mm).

Data Analysis

Dynamic MR angiograms were obtained by complex subtraction of selective and nonselective inversion-recovery true FISP images, and maximum intensity projection (MIP) images were then generated for each phase along three directions. The MIP images were displayed as a movie to visualize the flow of the labeled blood through the circle of Willis and its branches. Collapsed MIP images across

Table 1

Imaging Parameters in Three Experiments to Optimize TrueSTAR in 14 Healthy Volunteers

Parameter	Experiment 1 ($n = 4$)	Experiment 2 ($n = 4$)		Experiment 3 ($n = 6$)
		Part 2a	Part 2b	
Pulse sequence	2D TrueSTAR	3D TrueSTAR	Cardiac-gated 3D TrueSTAR	2D TrueSTAR and Look-Locker Echo-planar Imaging
Field of view (cm)	22 × 22	22 × 22	22 × 16.5	22 × 22
Matrix	256 × 256	256 × 256	224 × 162	256 × 256
Section thickness (mm)	5	2	1	6
No. of sections	8	20	64	7
Selective inversion band thickness (mm)	25, 50, 75	60	96	60
Repetition time/echo time (msec)	4/2	4/2	3/1.5	4/2
Flip angle (degrees)	40	30	30	20, 40, 60
No. of phases	60	30	10–15	38
Temporal resolution (msec)	50	83	52	65
Imaging time (min)	16	7*	6*	11

Note.—2D = two-dimensional.

* Generalized autocalibrating partially parallel acquisition with an acceleration factor of two.

all phases were also generated along axial, coronal, and sagittal views.

Arterial regions of interest primarily containing the middle cerebral artery and its main branches were first defined in user-specified regions on the collapsed MIP images (data collection and analysis performed by L.Y., S.W., Y.Y., Q.Z., and D.J.J.W., with a mean of 2 years experience) followed by automatic thresholding to eliminate the background signal. Dynamic time courses of the blood signal intensity as a function of inversion time were derived from the arterial regions of interest (mean size, 580 pixels ± 130). The SNR and contrast-to-noise ratio (CNR) efficiencies, determined as SNR and CNR, respectively, divided by the square root of acquisition time, were used to compare the performances of TrueSTAR and Look-Locker echo-planar imaging. The SNR was calculated as follows: SNR = SI_{art}/SD_{bg}, where SI_{art} is the mean signal intensity measured in the arterial region of interest and SD_{bg} is the standard deviation of the signal intensity in a region of interest in the background (mean size, 106 pixels ± 26). The CNR between the artery and adjacent soft tissue was calculated as follows: CNR = $(SI_{art} - SI_{tis})/SD_{bg}$, where SI_{tis} is the mean signal intensity measured in a region of interest in the adjacent soft tissue.

Statistical Analysis

Statistical analyses were performed by using software (SPSS, version 12.0; SPSS, Chicago, Ill). The values of SNR and CNR efficiency between TrueSTAR and Look-Locker echo-planar imaging at each flip angle tested ($\alpha = 20°$, 40°, and 60°) were compared by using the nonparametric Wilcoxon signed rank test. A two-tailed P value of .05 or less was considered to indicate a significant difference (without correction for multiple comparisons).

Results

Experiment 1: Optimization of Labeling Parameters

Figure 2a shows the mean dynamic MR angiography time course of the arterial regions of interest in four healthy subjects acquired with three different selective inversion bands (ie, 25, 50, and 75 mm) for a two-dimensional 5-mm-thick section. As expected, the bolus arrival was delayed with the thicker inversion band. The mean peak delays were 609 msec ± 178, 695 msec ± 202, and 767 msec ± 230 for the 25-, 50-, and 75-mm bands, respectively. The dynamic MR angiography signal intensities returned to baseline when the inversion time was greater than 2 seconds. A 10–20-mm gap between the labeling region and imaging sections was chosen for subsequent two-dimensional and 3D TrueSTAR imaging as the optimal tradeoff between providing adequate SNR and capturing the inflowing phases of dynamic MR angiography. The mean TrueSTAR dynamic MR angiography time course averaged for six subjects with three flip angles is shown in Figure 2b. The magnitudes of mean dynamic MR angiography time courses are roughly proportional to the sine of the flip angle (Fig 2c), suggesting little saturation effects of the TrueSTAR signal at large flip angles. (Note: data in Figure 2b and 2c were acquired in experiment 3.)

Experiment 2: Dynamic Visualization of Blood Flow

Figure 3 shows the axial, coronal, and sagittal views of the dynamic MR angiography MIP images acquired at different phases from a representative subject with 3D acquisitions with parallel imaging (experiment 2a). The full details of the dynamic courses of the labeled blood as it fills the circle of Willis and the main and small distal branches of the anterior, middle, and posterior cerebral arteries can be viewed in movies 1–3 (online).

Figure 4 shows the axial, coronal, and sagittal views of the dynamic MR angiography MIP images acquired by using pulse-gated 3D cine acquisitions (experiment 2b). Owing to the high resolution and large coverage in the section direction, the dynamic filling of the main branches of the anterior cerebral artery (segments A1 and A2), middle cerebral artery (segments M1, M2, and M3),

Figure 2

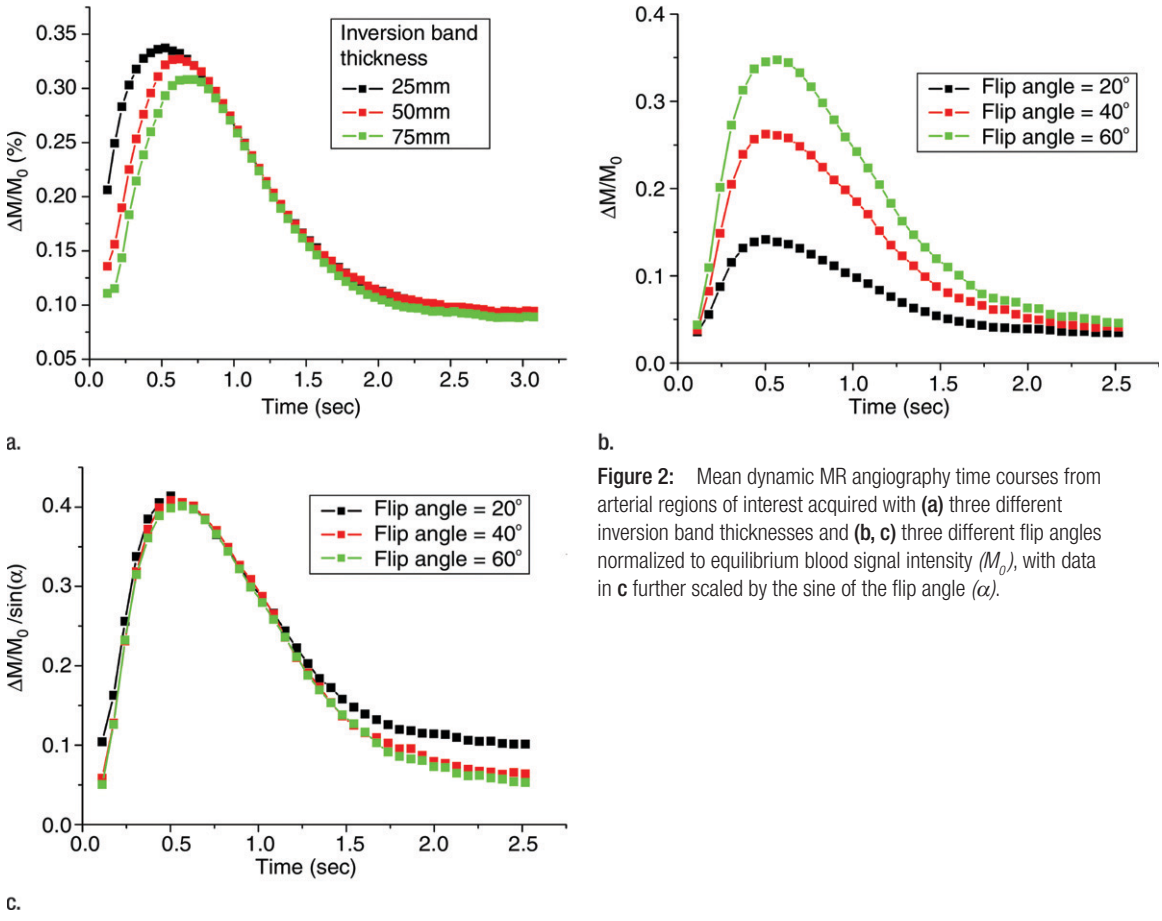

Figure 2: Mean dynamic MR angiography time courses from arterial regions of interest acquired with **(a)** three different inversion band thicknesses and **(b, c)** three different flip angles normalized to equilibrium blood signal intensity *(M_0)*, with data in **c** further scaled by the sine of the flip angle *(α)*.

and posterior cerebral artery (segments P1, P2, and P3) can be appreciated in coronal and sagittal views with greater detail compared with Figure 3 in each of the four subjects (movies 4–6 [online]). The drawback of the pulse-gated approach, however, was the relatively short cardiac cycle (~1 second) that only allowed a few phases to capture the inflowing and rising phases of the labeled blood.

Experiment 3: Comparison of Techniques

Figure 5 displays the results comparing the dynamic MR angiography data acquired by using two-dimensional TrueSTAR and Look-Locker echo-planar imaging. The values of SNR efficiency were, on average, 29% higher for TrueSTAR images than for Look-Locker echo-planar images for each of the three flip angles tested ($P = .028$) (Fig 5a and Table 2). The CNR efficiency values were 39% higher for TrueSTAR images than for Look-Locker echo-planar images ($P = .028$) (Table 2). Additionally, Figure 5b of the dynamic MR angiography collapsed MIP images shows ghost artifacts of the M1 segments of the middle cerebral artery along the phase encoding direction (anterior-posterior) on Look-Locker echo-planar images. These artifacts may be attributed to the pulsation effects of major arteries on segmented echo-planar imaging acquisitions. In contrast, the TrueSTAR images are not only artifact free but also provide detailed delineation of small arteries with great spatial resolution. Owing to the reduced sensitivity to field inhomogeneity effects, the TrueSTAR images also provide improved visualization of the anterior cerebral artery. The mean SNR efficiency of 3D TrueSTAR imaging (experiment 2) was 32.82 ± 2.65 with a flip angle of 30°, approximately four times that of two-dimensional TrueSTAR imaging with a similar flip angle, suggesting improved dynamic MR angiography image quality using 3D acquisitions with parallel imaging.

Dynamic MR Angiography in One Patient with an AVM

Figure 6 shows images of a 29-year-old man with an AVM located in the left occipitoparietal lobe. Dynamic MR angiography demonstrated the nidus and the feeding arteries, including the left posterior cerebral artery, left middle cerebral artery, and subsequent draining into the superficial venous system around the

Figure 3

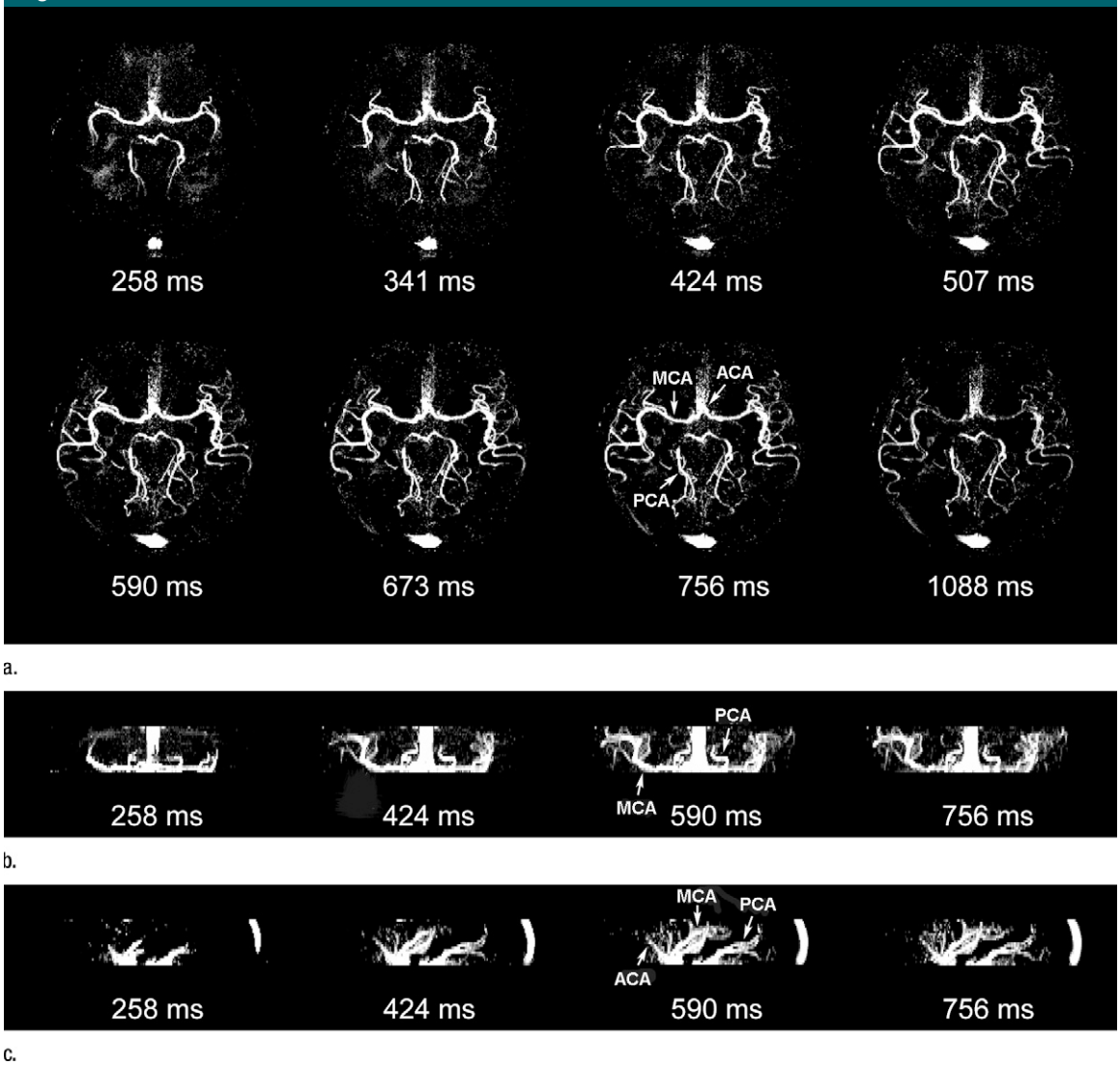

Figure 3: **(a)** Axial, **(b)** coronal, and **(c)** sagittal dynamic MR angiography MIP images acquired with 3D TrueSTAR from a representative subject. Note the anatomic details of dynamic courses for blood originating from internal carotid and basilar arteries as it fills the anterior cerebral artery *(ACA)*, middle cerebral artery *(MCA)*, and posterior cerebral artery *(PCA)* sequentially. Small branches of the middle cerebral artery and anterior and posterior cerebral arteries can also be seen in later phases of dynamic MR angiography. Note signal intensity in sagittal sinus owing to labeled venous blood superior to imaging sections. *ms* = milliseconds.

inversion time of 1500 msec. Although the draining vein overlaps with the nidus on the axial view, it can be clearly seen on coronal and sagittal views (Fig 6b and 6c), illustrating the importance for 3D acquisitions. The locations of the nidus and draining veins revealed by dynamic MR angiography matched well with those seen on time-of-flight MR angiography (Fig 6d). Nevertheless, TrueSTAR dynamic MR angiography provided temporal information (with a resolution of 50–100 msec) on the passage of labeled blood through the nidus and draining veins, allowing clear temporal separation of the feeding arteries from the draining veins (movies 7–9 [online]).

Discussion

Compared with existing spin-labeling–based dynamic MR angiography methods (10–13), the TrueSTAR technique offers improved SNR and CNR by capitalizing on the advantages of true FISP for flow imaging (eg, inherent flow compensation, high T2/T1 ratio of blood leading to improved SNR of labeled blood signal) (14,15). Image distortions owing to pulsation of arteries and flow-related signal voids in conventional Look-Locker echo-planar imaging–based dynamic MR angiography approaches are minimized by using TrueSTAR, especially with cardiac

Figure 4

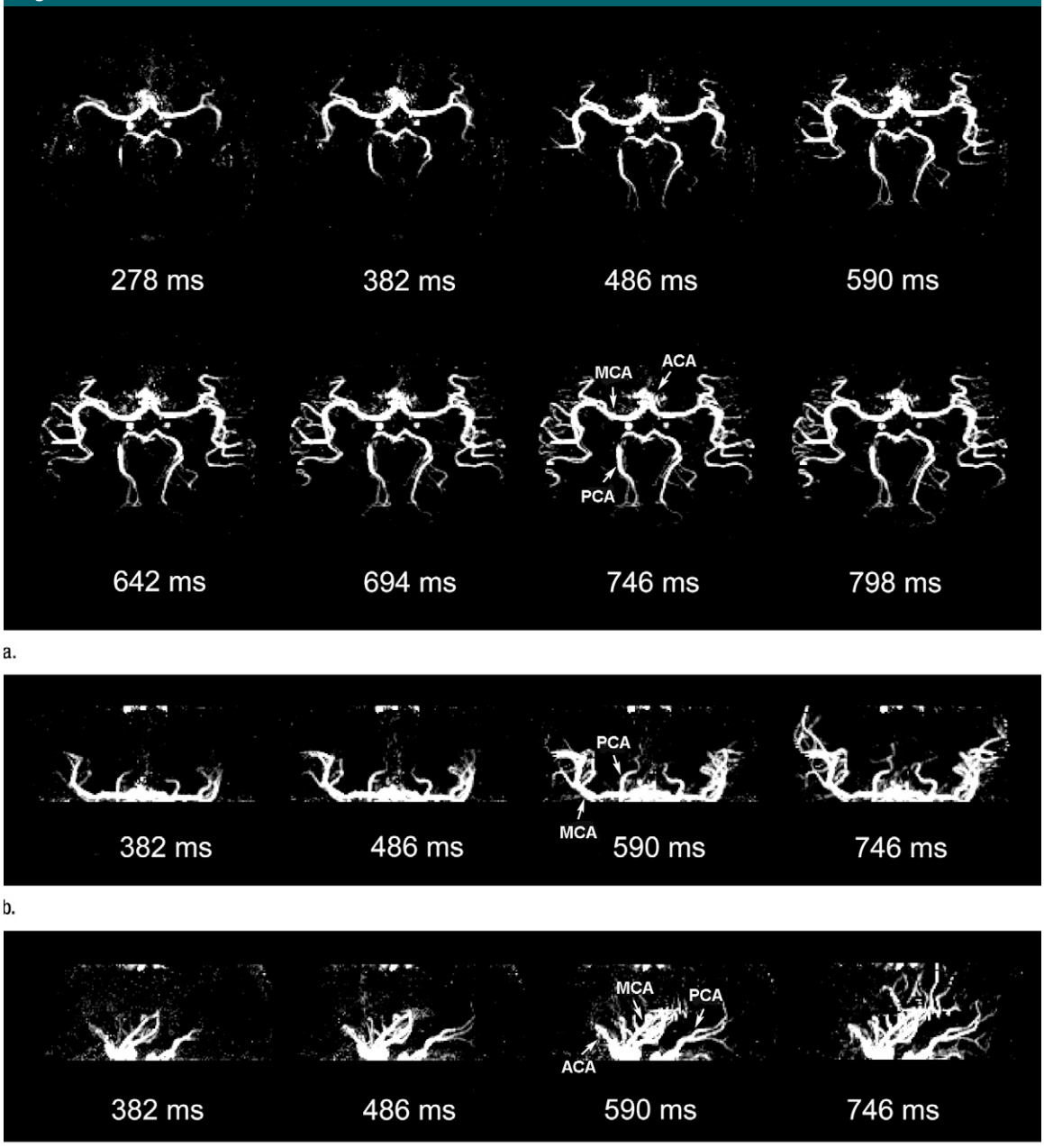

Figure 4: **(a)** Axial, **(b)** coronal, and **(c)** sagittal dynamic MR angiography MIP images acquired with 3D TrueSTAR by using a pulse-trigger in the same subject shown in Figure 3. Note improved sharpness. *ACA* = anterior cerebral artery, *MCA* = middle cerebral artery, *ms* = milliseconds, *PCA* = posterior cerebral artery.

gating. The through-plane resolution (1–3 mm) of TrueSTAR is also higher than that in the majority of existing unenhanced dynamic MR angiography methods owing to the use of 3D acquisitions and parallel imaging. Another potential advantage of TrueSTAR is that true FISP has relatively low sensitivity to magnetic field inhomogeneity effects compared with other fast imaging sequences, such as echo-planar imaging (17).

The total imaging time for TrueSTAR is determined by the temporal resolution (phases) and segments, as well as imaging coverage (sections). With the use of parallel imaging and partial Fourier acquisitions, we were

Figure 5

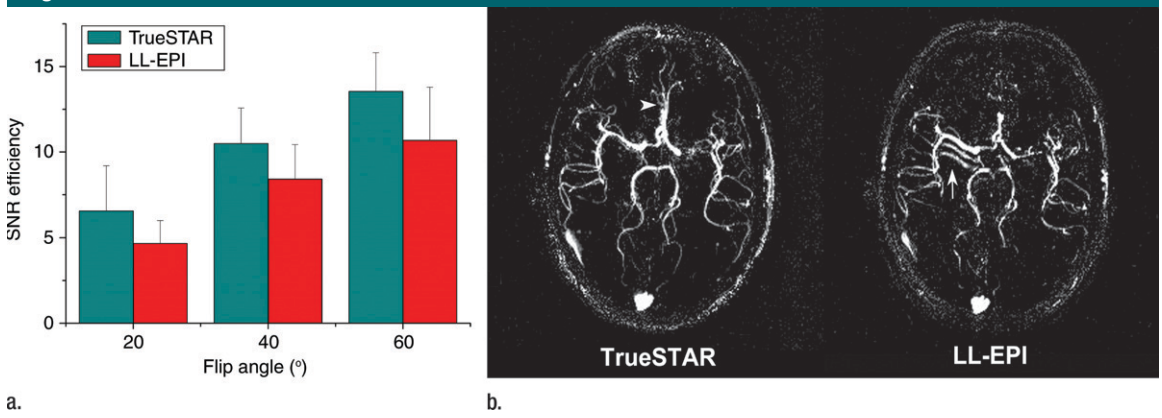

Figure 5: **(a)** Bar graph shows comparison of SNR efficiencies (SNR divided by square root of acquisition time) of dynamic MR angiography images between two-dimensional TrueSTAR and Look-Locker echo-planar imaging *(LL-EPI)* across three different flip angles. **(b)** Collapsed MIP images from a representative subject show ghost artifact in M1 segment of middle cerebral artery (arrow) on Look-Locker echo-planar image and improved visualization of anterior cerebral artery (arrowhead) on TrueSTAR image. SNR efficiency of 3D TrueSTAR is 32.82 ± 2.65.

Table 2

SNR and CNR Efficiencies at TrueSTAR or Look-Locker Echo-planar MR Imaging for Three Flip Angles

	TrueSTAR MR Imaging			Look-Locker Echo-planar MR Imaging		
Subject	20°*	40°*	60°*	20°*	40°*	60°*
	SNR Efficiency					
1	4.84	8.16	12.22	4.17	6.98	9.19
2	6.15	10.37	15.36	5.49	8.89	11.77
3	4.60	9.53	12.58	2.94	6.80	6.91
4	4.22	9.04	10.46	3.44	6.81	8.19
5	8.71	12.10	13.89	5.78	9.04	12.94
6	10.78	13.74	16.73	6.21	11.96	15.09
Mean†	6.55 ± 2.64	10.49 ± 2.08	13.54 ± 2.27	4.67 ± 1.34	8.41 ± 2.02	10.68 ± 3.11
	CNR Efficiency					
1	2.97	6.44	10.06	2.45	5.27	7.22
2	4.21	8.27	12.76	3.32	6.61	9.58
3	2.80	7.16	10.26	1.56	4.84	5.02
4	2.68	7.29	8.79	1.90	5.09	6.05
5	6.48	10.03	11.65	3.51	7.29	9.54
6	8.49	11.40	14.35	4.28	9.62	11.77
Mean†	4.60 ± 2.38	8.43 ± 1.90	11.31 ± 2.02	2.83 ± 1.04	6.45 ± 1.82	8.20 ± 2.53

Note.—SNR efficiency = $SNR/\sqrt{t}$. CNR efficiency = $CNR/\sqrt{t}$. t = imaging time.

* Flip angle.

† Data are means ± standard deviations.

able to develop a 3D imaging protocol with an imaging time of 6–7 minutes for clinical use. Cardiac-gated cine TrueSTAR acquisition allowed an isotropic 1-mm^3 spatial resolution and minimized cardiac pulsation effects on dynamic MR angiography images at the cost of fewer phases. The dynamic time courses of dynamic MR angiography signals offer the potential to estimate several flow-related parameters (eg, peak latency) and quantitative flow through a vessel of interest. Such capability may be clinically important to characterize the collateral flow pattern in steno-occlusive diseases, as well as to quantify shunted flow through an AVM.

The limitation of the TrueSTAR dynamic MR angiography technique is that the spatial resolution in the section direction (2–3 mm) is lower and the coverage is smaller (slab thickness, 40–60 mm) than those offered with standard contrast-enhanced dynamic MR angiography techniques. In the future, fast imaging approaches that have been successfully applied for contrast-enhanced dynamic MR angiography (eg, view sharing, keyhole, and undersampled radial acquisitions) can be applied for the TrueSTAR technique in conjunction with parallel imaging to further improve the spatiotemporal resolution and imaging coverage (22,23). One disadvantage of using flow-sensitive alternating inversion recovery for spin labeling is the potential contamination of labeled venous signals, which should be minimized by expanding the imaging slab and/or by applying a saturation band to saturate the venous signal. The newly introduced pseudocontinuous arterial spin labeling (24) offers more efficient spin labeling without venous contamination. In addition, TrueSTAR can be combined with vessel-selective labeling (25) for observing the dynamic inflowing pattern of a particular artery of interest. Finally, the clinical utility of

Figure 6

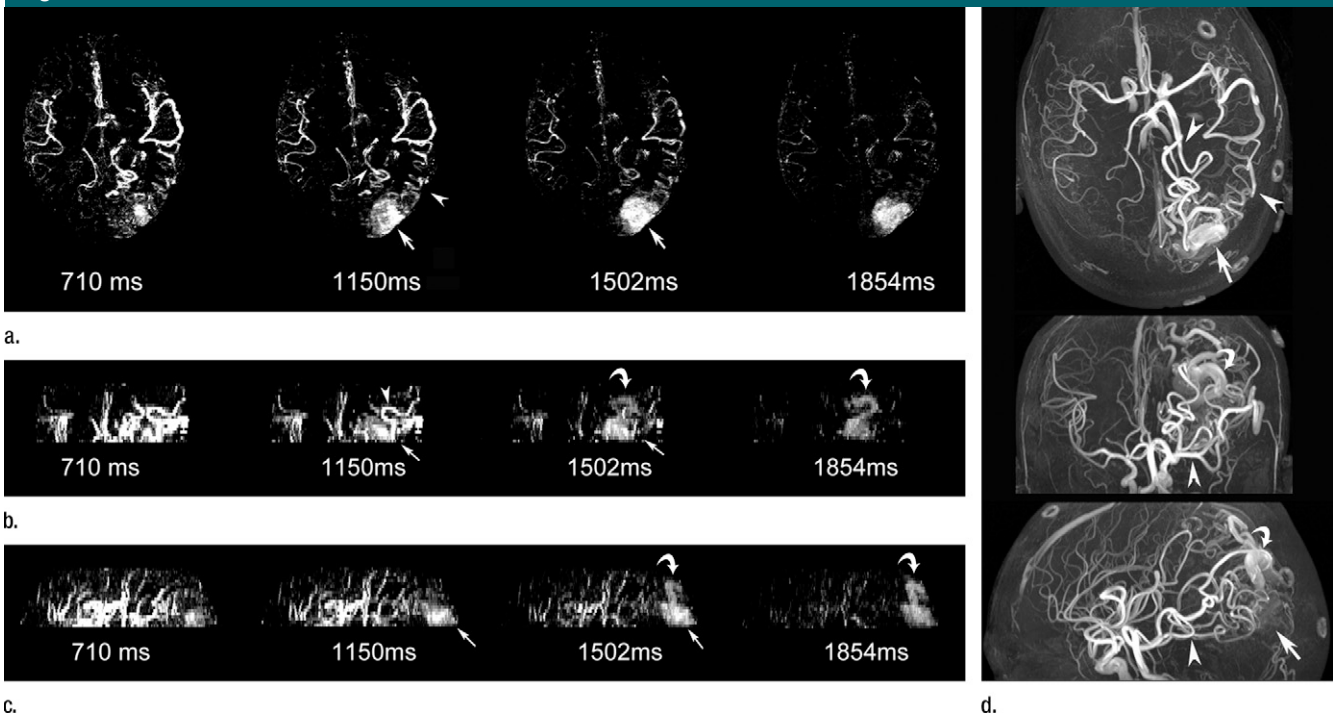

Figure 6: **(a)** Axial, **(b)** coronal, and **(c)** sagittal dynamic MR angiography MIP images of a 29-year-old man with AVM and **(d)** the associated MIP image of time-of-flight MR angiography. Arrowheads = feeding arteries. Arrows = nidus. Curved arrows = draining veins.

TrueSTAR needs to be determined in clinical evaluation studies.

In conclusion, a four-dimensional unenhanced dynamic MR angiography technique was introduced for visualizing the dynamic filling of the feeding arteries, nidus, and draining veins of AVM lesions with a spatial resolution of a few cubic millimeters and a temporal resolution of 50–100 msec.

Acknowledgments: The authors thank Jeroen Hendrikse, MD, PhD, (Department of Radiology, University Medical Center Utrecht, Utrecht, the Netherlands) for valuable comments and Bo Wang, MD, (Institute of Biophysics, Chinese Academy of Sciences) for assistance with data collection.

References

1. Wolf RL, Wang J, Detre JA, Zager EL, Hurst RW. Arteriovenous shunt visualization in arteriovenous malformations with arterial spin-labeling MR imaging. AJNR Am J Neuroradiol 2008;29(4):681–687.
2. Chng SM, Petersen ET, Zimine I, Sitoh YY, Lim CC, Golay X. Territorial arterial spin labeling in the assessment of collateral circulation: comparison with digital subtraction angiography. Stroke 2008;39(12):3248–3254.
3. Hollnagel DI, Summers PE, Poulikakos D, Kollias SS. Comparative velocity investigations in cerebral arteries and aneurysms: 3D phase-contrast MR angiography, laser Doppler velocimetry and computational fluid dynamics. NMR Biomed 2009;22(8):795–808.
4. Essig M, Engenhart R, Knopp MV, et al. Cerebral arteriovenous malformations: improved nidus demarcation by means of dynamic tagging MR-angiography. Magn Reson Imaging 1996;14(3):227–233.
5. Cloft HJ, Joseph GJ, Dion JE. Risk of cerebral angiography in patients with subarachnoid hemorrhage, cerebral aneurysm, and arteriovenous malformation: a meta-analysis. Stroke 1999;30(2):317–320.
6. Reinacher PC, Stracke P, Reinges MH, Hans FJ, Krings T. Contrast-enhanced time-resolved 3-D MRA: applications in neurosurgery and interventional neuroradiology. Neuroradiology 2007;49(suppl 1):S3–S13.
7. Ruhl KM, Katoh M, Langer S, et al. Time-resolved 3D MR angiography of the foot at 3 T in patients with peripheral arterial disease. AJR Am J Roentgenol 2008;190(6):W360–W364.
8. Griffin M, Grist TM, François CJ. Dynamic four-dimensional MR angiography of the chest and abdomen. Magn Reson Imaging Clin N Am 2009;17(1):77–90.
9. Lohan DG, Krishnam M, Tomasian A, Saleh R, Finn JP. Time-resolved MR angiography of the thorax. Magn Reson Imaging Clin N Am 2008;16(2):235–248.
10. Edelman RR, Siewert B, Adamis M, Gaa J, Laub G, Wielopolski P. Signal targeting with alternating radiofrequency (STAR) sequences: application to MR angiography. Magn Reson Med 1994;31(2):233–238.
11. van Osch MJ, Hendrikse J, Golay X, Bakker CJ, van der Grond J. Non-invasive visualization of collateral blood flow patterns of the circle of Willis by dynamic MR angiography. Med Image Anal 2006;10(1):59–70.
12. Warmuth C, Rüping M, Förschler A, et al. Dynamic spin labeling angiography in extracranial carotid artery stenosis. AJNR Am J Neuroradiol 2005;26(5):1035–1043.
13. Sallustio F, Kern R, Günther M, et al. Assessment of intracranial collateral flow by using dynamic arterial spin labeling MRA

and transcranial color-coded duplex ultrasound. Stroke 2008;39(6):1894–1897.

14. Carr JC, Simonetti O, Bundy J, Li D, Pereles S, Finn JP. Cine MR angiography of the heart with segmented true fast imaging with steady-state precession. Radiology 2001;219(3):828–834.

15. Merrifield R, Keegan J, Firmin D, Yang GZ. Dual contrast TrueFISP imaging for left ventricular segmentation. Magn Reson Med 2001;46(5):939–945.

16. Miyazaki M, Lee VS. Nonenhanced MR angiography. Radiology 2008;248(1):20–43.

17. Boss A, Martirosian P, Klose U, Nägele T, Claussen CD, Schick F. FAIR-TrueFISP imaging of cerebral perfusion in areas of high magnetic susceptibility differences at 1.5 and 3 Tesla. J Magn Reson Imaging 2007;25(5):924–931.

18. Yan L, Zhuo Y, Wang J. Quantitative dynamic MR angiography using ASL based TrueFISP [abstr]. In: Proceedings of the 17th meeting of the International Society for Magnetic Resonance in Medicine. Berkeley, Calif: International Society for Magnetic Resonance in Medicine, 2009; 3635.

19. Kim SG. Quantification of relative cerebral blood flow change by flow-sensitive alternating inversion recovery (FAIR) technique: application to functional mapping. Magn Reson Med 1995;34(3):293–301.

20. Le Roux P. Simplified model and stabilization of SSFP sequences. J Magn Reson 2003;163(1):23–37.

21. Bi X, Weale P, Schmitt P, Zuehlsdorff S, Jerecic R. Non-contrast-enhanced 4D intracranial MR angiography with 4D NATIVE TrueFISP [abstr]. In: Proceedings of the 17th meeting of the International Society for Magnetic Resonance in Medicine. Berkeley, Calif: International Society for Magnetic Resonance in Medicine, 2009; 3259.

22. Fink C, Ley S, Kroeker R, Requardt M, Kauczor HU, Bock M. Time-resolved contrast-enhanced three-dimensional magnetic resonance angiography of the chest: combination of parallel imaging with view sharing (TREAT). Invest Radiol 2005;40(1):40–48.

23. Mistretta CA. Undersampled radial MR acquisition and highly constrained back projection (HYPR) reconstruction: potential medical imaging applications in the post-Nyquist era. J Magn Reson Imaging 2009;29(3):501–516.

24. Dai W, Robson PM, Shankaranarayanan A, Alsop DC. MR cerebral angiography using arterial spin labeling for dynamic inflow visualization and vessel selectivity [abstr]. In: Proceedings of the 17th meeting of the International Society for Magnetic Resonance in Medicine. Berkeley, Calif: International Society for Magnetic Resonance in Medicine, 2009; 275.

25. Hendrikse J, van der Grond J, Lu H, van Zijl PC, Golay X. Flow territory mapping of the cerebral arteries with regional perfusion MRI. Stroke 2004;35(4):882–887.